

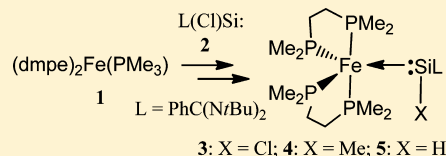
Electron-Rich N-Heterocyclic Silylene (NHSi)–Iron Complexes: Synthesis, Structures, and Catalytic Ability of an Isolable Hydridosilylene–Iron Complex

Burgert Blom, Stephan Enthaler, Shigeyoshi Inoue,* Elisabeth Irran, and Matthias Driess*

Department of Chemistry: Metalorganics and Inorganic Materials, Technische Universität Berlin, Strasse des 17. Juni 135, Sekr. C2, D-10623 Berlin, Germany

Supporting Information

ABSTRACT: The first electron-rich N-heterocyclic silylene (NHSi)–iron(0) complexes are reported. The synthesis of the starting complex is accomplished by reaction of the electron-rich Fe^0 precursor $[(\text{dmpe})_2\text{Fe}(\text{PMe}_3)]$ **1** (dmpe = 1,2-bis(dimethylphosphino)ethane) with the N-heterocyclic chlorosilylene LSiCl ($\text{L} = \text{PhC}(\text{N}^t\text{Bu})_2$) **2** to give, via Me_3P elimination, the corresponding iron complex $[(\text{dmpe})_2\text{Fe}(\leftarrow\text{Si}(\text{Cl})\text{L})]$ **3**. Reaction of in situ generated **3** with MeLi afforded $[(\text{dmpe})_2\text{Fe}(\leftarrow\text{Si}(\text{Me})\text{L})]$ **4** under salt metathesis reaction, while its reaction with $\text{Li}[\text{BHEt}_3]$ yielded $[(\text{dmpe})_2\text{Fe}(\leftarrow\text{Si}(\text{H})\text{L})]$ **5**, a rare example of an isolable Si^{II} hydride complex and the first such example for iron. All complexes were fully characterized by spectroscopic means and by single-crystal X-ray diffraction analyses. DFT calculations further characterizing the bonding situation between the Si^{II} and Fe^0 centers were also carried out, whereby multiple bonding character is detected in all cases (Wiberg Bond Index >1). For the first time, the catalytic activity of a Si^{II} hydride complex was investigated. Complex **5** was used as a precatalyst for the hydrosilylation of a variety of ketones in the presence of $(\text{EtO})_3\text{SiH}$ as a hydridosilane source. In most cases excellent conversions to the corresponding alcohols were obtained after workup. The reaction pathway presumably involves a ketone-assisted 1,2-hydride transfer from the Si^{II} to Fe^0 center, as a key elementary step, resulting in a betaine-like silyliumylidene intermediate. The appearance of the latter intermediate is supported by DFT calculations, and a mechanistic proposal for the catalytic process is presented.

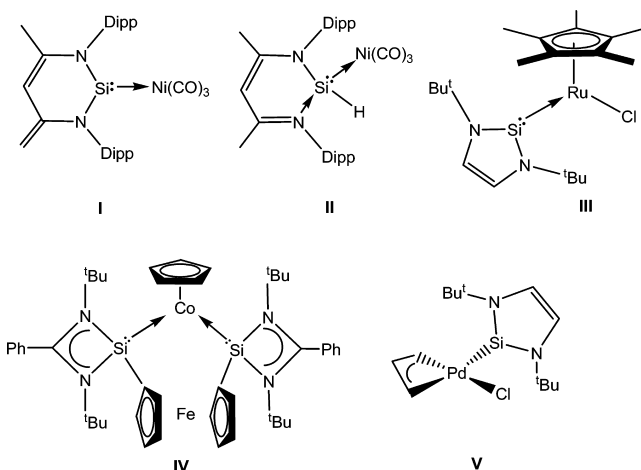


INTRODUCTION

Since the seminal work of Schmid and Wels in 1977, who reported the first N-heterocyclic silylene (NHSi) complex,¹ a plethora of NHSi complexes have been reported for a large array of the transition metal elements.² Burgeoning interest, in our and other groups, in these complexes has been further precipitated by recent reports highlighting their use in a variety of small molecule activations (NH_3 , H_2S , hydrazines etc.; **I**, Chart 1),³ interesting stoichiometric transformations, for example hydrosilylation of alkynes (**II**, Chart 1),⁴ or silane activation (**III**, Chart 1).⁵ Moreover they have been demonstrated to be active in a variety of catalytic transformations such as $[2 + 2 + 2]$ cycloaddition of substituted alkynes (**IV**, Chart 1),⁶ Suzuki cross coupling of aryl boronic acids with bromoarenes,⁷ Heck coupling of styrene and bromoacetophenone (**V**, Chart 1),⁸ and the recently reported borylation of arenes,⁹ clearly demonstrating their potential and spurring on further development.

An abundance of synthetic routes enabling access to NHSi complexes now exist, mostly involving ligand elimination reactions (CO ,¹⁰ thf ,¹¹ cod (1,5-cycloocta-1,3-diene),¹² PPh_3 ,¹³ PEt_3 ,¹⁴ or even N-heterocyclic carbenes¹⁵) from suitable transition metal precursors upon reaction with “free” NHSis.² We recently showed that a PMe_3 elimination strategy can even enable facile entry to novel titanium NHSis complexes of the type $[(\text{C}_5\text{H}_5)_2\text{Ti}(\leftarrow\text{SiXL})_2]$ ($\text{L} = \text{PhC}(\text{N}^t\text{Bu})_2$, $\text{X} = \text{Cl}$,

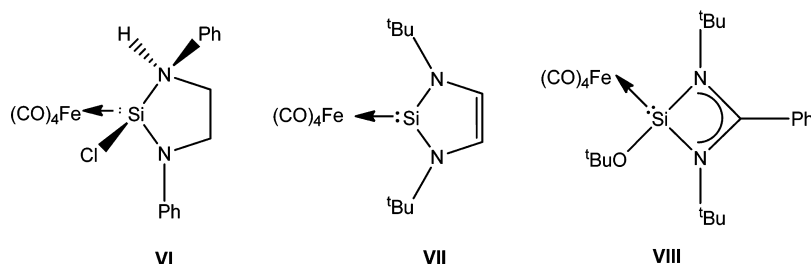
Chart 1. Examples of Recently Reported NHSi Complexes Active in Various Stoichiometric or Catalytic Transformations



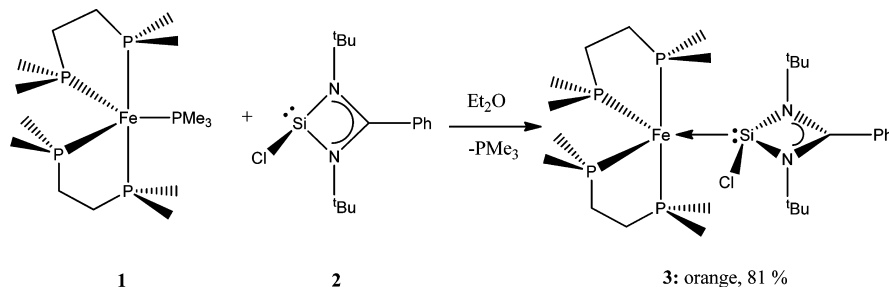
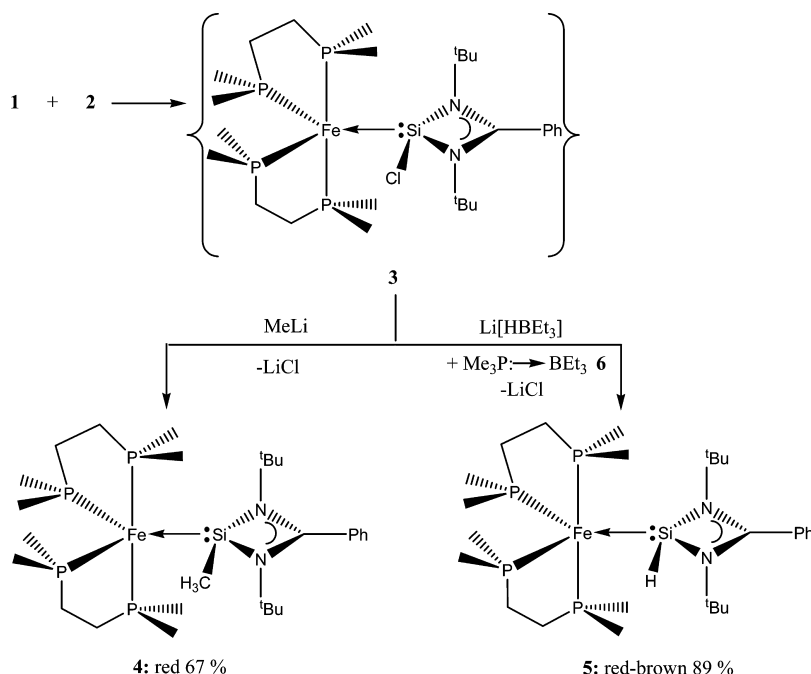
CH_3 , H), representing the first examples of group IV NHSi complexes.¹⁶

Received: March 13, 2013

Chart 2. Previously Known Fe–NHSi Complexes



Scheme 1. Synthesis of Electron-Rich Fe–NHSi Complex 3

Scheme 2. Synthesis of 4 and 5 by in Situ Generation of 3 and Subsequent Reaction with MeLi or Li[HBEt₃], Respectively

With a view of exploring the generality of this PMe_3 elimination route to access NHSi complexes of other transition metals and exploring their inherent reactivity and catalytic activity, we became interested in exploring an analogous route to access iron NHSis, which are surprisingly rare. To date, the few existing iron–NHSi complexes exclusively bear the $\{\text{Fe}(\text{CO})_4\}$ fragment (Chart 2).^{1,17,18} The probable reason for this is a lack of suitable iron precursors to access other NHSi iron complexes. With this in mind, we considered the complex $[(\text{dmpe})_2\text{Fe}(\text{PMe}_3)]$ (dmpe = 1,2-bis(dimethylphosphino)ethane) (**1**) as a possible starting material previously shown to be a suitable precursor in accessing iron–Group 14 element (Ge and Sn) multiple bonds, by PMe_3 elimination.¹⁹ We reasoned that by increasing the electron

density at the iron center with electron pushing alkyl phosphane ligands as opposed to CO ligands, enhanced π -back-bonding to the Si^{II} center should result, potentially increasing the reactivity of the overall complex, which is desirable in a catalytic context. Surprisingly, no previous reports exist where Fe-based silylene complexes²⁰ have been used in catalysis, and given the extremely low cost and abundance of iron, we felt further warranted investigation.

Herein we report the first examples of electron-rich Fe–NHSi complexes, obtained by a PMe_3 elimination strategy, and their reactivity. Moreover, the first catalytic investigations on any Fe-based NHSi or Si^{II} hydrido complex are reported, showcasing the potential of reactive Si^{II} hydrides in catalysis.

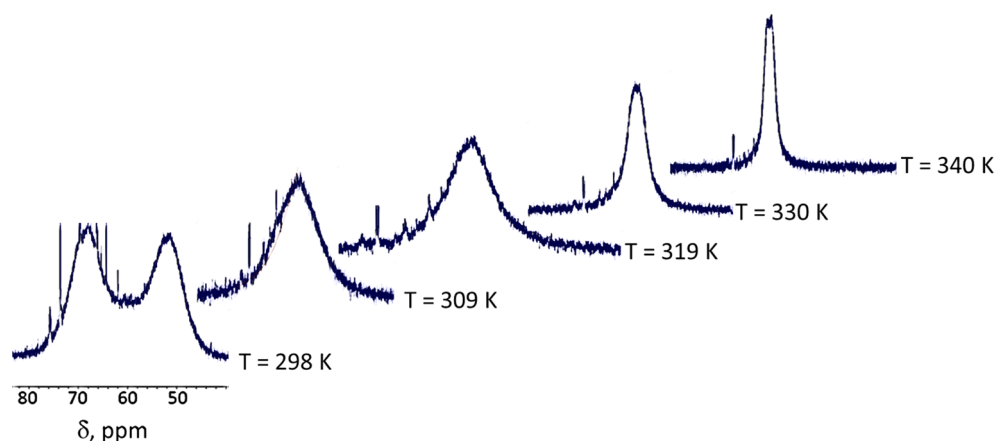


Figure 1. Stacked variable temperature (VT) $^{31}\text{P}\{^1\text{H}\}$ NMR spectra of the hydrido-NHSi complex **5** revealing two bands at 298 K collapsing into a broad signal at 309 K with concomitant signal sharpening on temperature ascent due to the onset of pseudorotation (measured in C_6D_6 at 161.9 MHz).

RESULTS

Reaction of the electron-rich Fe^0 precursor $[(\text{dmpe})_2\text{Fe}(\text{PMe}_3)]$ (**1**)¹⁹ with the intramolecularly N-donor-stabilized chlorosilylene LSiCl ($\text{L} = \text{PhC}(\text{N}^t\text{Bu})_2$) (**2**)²¹ in diethyl ether affords, with concomitant PMe_3 elimination, the extremely air sensitive orange complex $[(\text{dmpe})_2\text{Fe}(\leftarrow\text{Si}(\text{Cl})\text{L})]$ (**3**) in 81% yield (Scheme 1). Complex **3** is a rare example of an NHSi complex of Fe, and can be considered much more electron-rich than the previously reported $[\text{Fe}(\text{CO})_4]$ complexes due to the presence of electron pushing alkylphosphane donor ligands.

Owing to the stabilization of the reactive Si^{II} center by the $\{\text{FeP}_4\}$ fragment in complex **3**, further reactions can be carried out at the Si^{II} center. For example, in situ generation of **3** followed by reaction with MeLi afforded, by metathetical exchange at the silicon center, the complex $[(\text{dmpe})_2\text{Fe}(\leftarrow\text{Si}(\text{Me})\text{L})]$ (**4**), in 67% yield as a red solid (Scheme 2). Furthermore, the reaction of in situ generated **3** with $\text{Li}[\text{HBEt}_3]$ afforded by halide–hydride exchange a mixture of $[(\text{dmpe})_2\text{Fe}(\leftarrow\text{Si}(\text{H})\text{L})]$ (**5**) and $\text{Me}_3\text{P} \rightarrow \text{BEt}_3$ (**6**). The desired complex **5** could be separated from **6** by crystallization, affording **5** in 89% yield as a red-brown solid (Scheme 2). Isolable Si^{II} hydrides are very rare due to their concomitant high reactivity,²² and generally require stabilization by a transition metal complex fragment or intramolecular donor–acceptor stabilization. Complex **5** is the first example of an isolable hydrido– Si^{II} complex of iron. Strikingly, complexes **3**–**5** are all thermally very stable with decomposition temperatures well above 110 °C, a desirable property to probe their suitability as precatalysts for organic transformations.

Complexes **3** and **4** feature relatively broad signals (**3**: $\Delta\nu_{1/2} = 58.1$ Hz; **4**: $\Delta\nu_{1/2} = 48.6$ Hz) in their $^{31}\text{P}\{^1\text{H}\}$ NMR spectra at room temperature both at ca. δ 60 ppm, suggesting slow exchange of P_{ax} and P_{eq} atoms on NMR time scale facilitated by Berry pseudorotation.^{23,24} The broadness of the signals is likely due to the close proximity of the exchange process to the coalescence temperature, below which the pseudorotation would be completely frozen out into two distinct signals. This is clearly demonstrated in complex **5**, which features two very broad signals in the $^{31}\text{P}\{^1\text{H}\}$ NMR spectrum at room temperature at the same measuring frequency (161.9 MHz) at δ 51.5 ($\Delta\nu_{1/2} = 1503$ Hz) and δ 67.9 ($\Delta\nu_{1/2} = 1503$ Hz), indicative of frozen out Berry pseudorotation and a static structure. The $^{31}\text{P}\{^1\text{H}\}$ NMR spectrum of **5** at ambient

temperature, at a lower measuring frequency (80 MHz), however, shows only one very broad signal pointing to very slow fluxional exchange of the P atoms at the lower frequency, in accordance with expectations.²⁵ At higher temperatures, the $^{31}\text{P}\{^1\text{H}\}$ NMR spectra of **5** reveal a broad signal at 309 K (δ 59.5 ppm, ($\Delta\nu_{1/2} = 2236$ Hz)), with concomitant signal sharpening on increased temperature (330 K, δ 60.3 ppm, $\Delta\nu_{1/2} = 902$ Hz) (Figure 1). The coalescence temperature for P exchange thus lies between 298 and 309 K at this measuring frequency (161.9 MHz) in complex **5**. These findings reveal an increase in the energy barrier associated with the Berry pseudorotation of the dmpe ligands in complex **5**, compared to **3** and **4**. This observation cannot be accounted for on steric grounds since **5** features the smallest substituent (H) on Si compared to **3** (Cl) and **4** (CH_3). Wilson and co-workers have documented a relationship between the energy barrier of the pseudorotation and the π -accepting ability of the alkene in complexes of the type $[\text{Fe}(\text{CO})_4(\text{alkene})]$, where a π -acidic alkene exhibits a higher pseudorotational energy barrier.²⁶ In accordance with these findings, in our case the: $\text{Si}(\text{L})\text{H}$ ligand may exhibit a higher π -accepting ability in **5** compared to: $\text{Si}(\text{L})\text{Cl}$ (**3**) or: $\text{Si}(\text{L})\text{Me}$ (**4**), which was investigated by DFT studies (see below).

The ^1H NMR spectra (400 MHz) of **3** and **4** at room temperature exhibit two sets of diastereotopic signals (CH_3^{A} and CH_3^{B}) for the methyl groups of the dmpe ligands, in accordance with the fluxional picture observed in the $^{31}\text{P}\{^1\text{H}\}$ NMR spectra (complex **4** exhibits an additional signal for the $\text{Si}-\text{CH}_3$ group). Due to the frozen out Berry pseudorotation at ambient temperatures in **5**, four diastereotopic CH_3 groups (CH_3^{A} , CH_3^{B} , CH_3^{C} , CH_3^{D}) are observed as expected (at measuring frequency of 400 MHz). These four signals also coalesce into two bands at higher temperatures ($T \geq 309$ K), resulting in spectra resembling those of **3** and **4** at room temperature, in accordance with the observations in the VT $^{31}\text{P}\{^1\text{H}\}$ spectra, also confirming pseudorotation at higher temperatures.²⁷ A key feature in complex **5** is the presence of the Si–H signal, which at room temperature is not clearly distinguishable and obscured by aromatic resonance signals. The signal could unambiguously be located in the ^1H NMR spectrum by use of a 2D (^1H , ^{29}Si) heteronuclear shift correlation experiment at δ 6.85 ppm, providing additional evidence of its connectivity to Si. At higher temperatures ($T \geq$

309 K), the Si–H signal is clearly visible as a quintet (δ 6.85 ppm, $^3J_{\text{HP}} = 9.9$ Hz), the quintet multiplicity deriving from coupling to the phosphorus atoms rendered equivalent at this temperature by the ensuing pseudorotation *vide supra* (Figure 2).

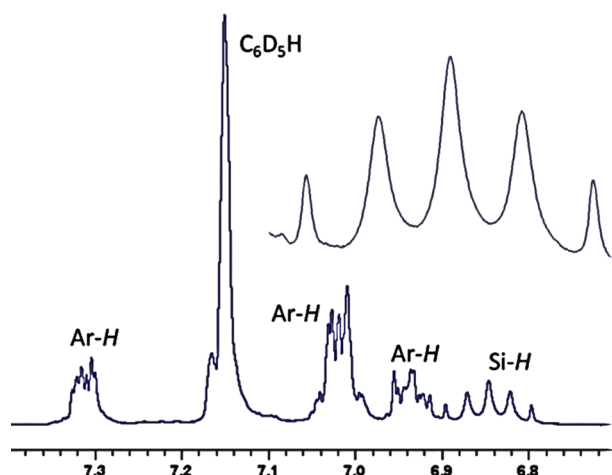


Figure 2. ^1H NMR spectrum (400 MHz) of **5** in C_6D_6 at 340 K in the aromatic region with an enlargement of the Si–H resonance signal showing its quintet multiplicity derived from $^3J_{\text{PH}}$ coupling.

The $^{29}\text{Si}\{^1\text{H}\}$ NMR shifts of complexes **3**–**5** were also recorded, and in each case feature a quintet multiplicity, resulting from a $^2J_{\text{SiP}}$ coupling to four equivalent P atoms (rendered equivalent by Berry pseudorotation) on NMR time scale for ^{29}Si (Table 1).

Table 1. $^{29}\text{Si}\{^1\text{H}\}$ NMR Data and Hammett Constants for Complexes **3**–**5**

complex, (Si–X)	$^{29}\text{Si}\{^1\text{H}\}$ NMR δ value (ppm)	$^2J_{\text{SiP}}$ coupling constant (Hz)	Hammett constant (σ_p)
3 (X = Cl)	43.1	12.1	0.23
4 (X = CH_3)	102.5	16.1	–0.17
5 (X = H)	63.6	23.7	0

Inspection of the $^{29}\text{Si}\{^1\text{H}\}$ NMR chemical shifts (δ values) of complexes **3**–**5** reveals a negative linear relationship between chemical shift and Hammett constant (σ_p)²⁸ of the substituents that is evidence that inductive and resonance effects of the substituents are a factor in the ^{29}Si chemical shift position. The same trend was observed for an analogous series of Ti^{II} NHSi complexes, bearing the same substituents on Si,¹⁶ and can be explained on the basis of the Bent rule.²⁹ The shielding of the silicon nucleus in **3** results from a concentration of p-character in the Si–Cl bond, which concomitantly results in increased s-character in the contribution of the silicon atom of the iron silicon bond. This increase in the s-character results in a shielding effect and the lower chemical shift value. Conversely, in the case of **4** the exact opposite can be expected on the basis of the Bent rule, and a lower s-character in the contribution of the silicon atom in the silicon iron bond is predicted, resulting in deshielding and a larger chemical shift. This was confirmed on the basis of bonding analysis of the Si–Fe bond (*vide infra*).

Suitable crystals for X-ray diffraction analyses of **3**–**5** were obtained by slow cooling of saturated solutions (**3**: Et_2O ; **4**, **5**: *n*-hexane) to -30 °C for several days. The molecular structures

of all three compounds reveal slightly distorted trigonal-bipyramidal coordination geometries around the iron centers (**3**: $\tau = 0.87$; **4**: $\tau = 0.82$; **5**: $\tau = 0.95$)³⁰ with the NHSi ligand occupying one of the equatorial coordination sites in each case. This is the typically preferred position for π -accepting ligands in a trigonal-bipyramidal geometry, which provides some evidence for the π -accepting ability of the NHSi ligand. The structure solution of complex **5** was complicated by substantial statistical disorder over the dmpe bridges, which could, however, be resolved in a satisfactory fashion by solving (number of restraints = 484) for the coexistence of two stereoisomers. The origin of this disorder is likely caused by the increased energy barrier of pseudorotation observed spectroscopically, which resulted during crystallization in the formation of two coexisting stereoisomers, in a ratio of 1:1. Figures 3 – 5

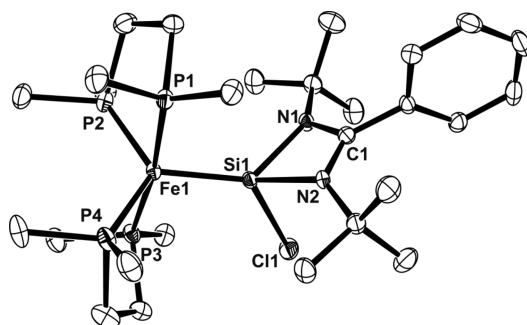


Figure 3. ORTEP representation of the molecular structure of **3**. Hydrogen atoms are omitted for clarity, thermal ellipsoids set at 30% probability. Selected distances [Å] and angles [deg]: Fe1–P1 2.166(2), Fe1–P2 2.156(2), Fe1–P3 2.153(3), Fe1–P4 2.148(3); P1–Fe1–P2 171.48(10), P1–Fe1–P3 93.22(11), P2–Fe1–P4 92.89(11), P4–Fe1–P3 122.45(11), P4–Fe1–Si1 118.46(10), P3–Fe1–Si1 119.09(10), P2–Fe1–Si1 93.81(9), P1–Fe1–Si1 94.67(9).

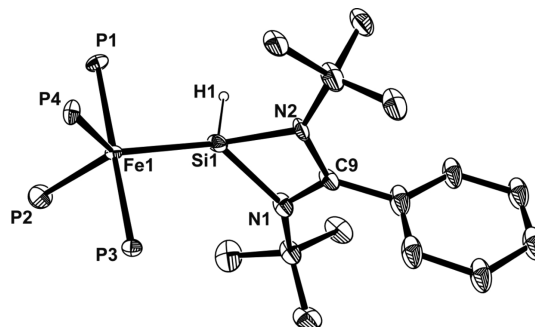


Figure 4. ORTEP representation of the molecular structure of **5**. All carbon atoms on dmpe ligands and H atoms omitted for clarity (except H1), thermal ellipsoids set at 30% probability. Selected distances [Å] and angles [deg]: Fe1–P1 2.156(9), Fe1–P2 2.123(12), Fe1–P3 2.161(18), Fe1–P4 2.193(8); P1–Fe1–P2 88.7(3), P2–Fe1–P3 91.7(4), P1–Fe1–P3 179.6(5), P2–Fe1–P4 113.0(4), P2–Fe1–Si1 123.9(4), P1–Fe1–Si1 86.5(2).

show the molecular structures of complexes **3** and **5** in the solid state (for the structure of **4** see the Supporting Information). Figure 5 shows the resolved disorder over the dmpe bridges resulting from the coexistence of two stereoisomers.

The Fe–Si distances for the three complexes range from 2.1634(9) Å in **3** to 2.200(2) Å in **4**, with complex **5** exhibiting a value of 2.184(2) Å (Table 2). The observed Fe–Si lengths correlate perfectly with the Hammett constants (σ_p) associated

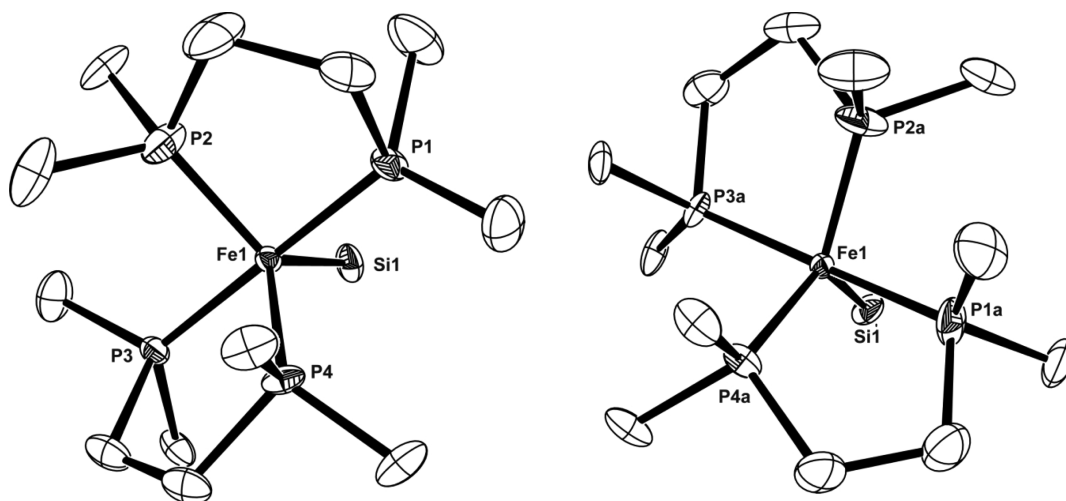


Figure 5. ORTEP representations of complex **5** showing the disorder over the dmpe bridges, resolved as two stereoisomers. The two stereoisomers were found in approximately 1:1 ratio, accounting for the disorder. Thermal ellipsoids set at 30% probability, H atoms and all substituents on Si omitted for clarity.

Table 2. Selected Distances for the Complexes 3–5^a

	$d(\text{Fe}–\text{Si})/\text{\AA}$	$d(\text{Si}–\text{X})/\text{\AA}$	$d(\text{Si}–\text{N1})/\text{\AA}$	$d(\text{Si}–\text{N2})/\text{\AA}$
3	2.1634(9)	2.2281(11)	1.920(2)	1.931(2)
4	2.200(2)	1.933(9)	1.954(7)	1.948(7)
5	2.184(2)	1.50(2) ^b	1.930(6)	1.915(7)

^aX = Cl (**3**), CH₃ (**4**), H (**5**). ^bThe H atom attached to Si in **5** could not be located experimentally and was constrained at a distance of 1.50(2) Å.

with the substituents on the Si^{II} centers in analogy to the trend observed with the respective ²⁹Si NMR shifts of **3**–**5** vide supra. This is an additional indication of the influence of the substituent on the nature of the Fe–Si bond. Furthermore, these bond lengths are slightly shorter when compared to the only two existing Fe–NHSi complexes reported to date: 2.196 Å (**VII**) and 2.237 Å (**VIII**) (Chart 2). This observation is likely due to the increased electron density at the Fe centers in **3**–**5** resulting from electron pushing alkyl phosphane ligands, as opposed to good σ -donor and additionally strong π -acceptor ability of the CO ligands in **VII** and **VIII**, facilitating stronger π -back-donation to the Si^{II} centers and concomitant bond length contraction. The Fe–Si distances are in fact comparable to that of the donor-free silylene complex $[(\eta^5\text{-C}_5\text{Me}_5)_2\text{Fe}(\text{CO})-(\text{SiMe}_3)(=\text{SiMe}_2)]$ (Mes = 2,4,6-Me₃-C₆H₂) by Tobita and co-workers, where a formal double bonding interaction between iron and silicon is observed,³¹ suggesting double bond character in **3**–**5**.

DFT Calculations. DFT calculations of the complexes **3**–**5**,³² including Natural Bond Orbital (NBO) analysis, were also performed particularly to elucidate the nature of the bonding interaction between the Si and Fe centers. A reasonable agreement exists for the Fe–Si bond lengths found in the geometry optimized structures with those observed by X-ray structure determinations (**3**: 2.179 Å; **4**: 2.226 Å; **5**: 2.198 Å). A summary of some pertinent metrical parameters for the DFT calculations of **3**–**5** is presented in Table 3.

The calculated NBO charges on the Fe and Si atoms in complexes **3** and **4** are comparable to each other within narrow limits, and point to highly polarized Fe–Si bonds in both complexes (Table 4). The NBO charge on Si in complex **5** is slightly less positive, possibly as a result of enhanced π -back-

Table 3. Comparison of Wiberg Bond Indices (WBI) Values and the Calculated Fe–Si Distances of Complexes 3–5^a

complex	NBO charge		WBI	Fe–Si distances (Å) ^b
	Fe	Si		
3	−2.205	+1.462	1.1934	2.1794 (2.1634)
4	−2.180	+1.531	1.1420	2.2259 (2.184)
5	−2.198	+1.237	1.1585	2.1976 (2.200)

^aLevel of theory: B3LYP/6-31G(d) for C, H, N, Cl and Si; LANL2DZ for Fe. ^bExperimental values by X-ray diffraction analysis in parentheses.

Table 4. NBO Analysis of the Fe–Si Bond^a

complex	bond polarization (%)	s-character (%)	p-character (%)	d-character (%)
3	Fe (33.79)	22.30	69.28	8.51
	Si (66.21)	84.52	15.48	0.01
4	Fe (37.02)	22.18	67.55	10.28
	Si (62.98)	61.49	38.46	0.05
5	Fe (36.54)	21.48	66.93	12.22
	Si (63.46)	64.94	35.05	0.02

^aLevel of theory: B3LYP/6-31G(d) for C, H, N, Cl and Si; LANL2DZ for Fe.

donation from the Fe⁰ center to Si^{II}. The calculated Wiberg bond index (WBI)³³ of all three complexes is >1, which is clear evidence of multiple bonding character in the Fe–Si bonds.³⁴ Figure 6 shows the distribution of the energies and shapes of the frontier MOs of complex **3**, which were found to be very similar in complex **4**.

Inspection of the calculated MOs for complexes **3** and **4** reveals that the HOMO has an asymmetric distribution of electron density resulting from the π -back-donation from the Fe⁰→Si^{II} while the HOMO-1 and HOMO-2 MOs also reflect a potential π -interaction between the Fe and Si centers, since their shape reveals somewhat polarized metal d-orbitals. The presence of the electron pushing alkylphosphane ligands enhances the electron density at the iron center, and facilitates π -back-bonding to silicon. This is in contrast to other examples of NHSi complexes bearing the {Fe(CO)₄} fragment, where the π -acidity of the CO ligands should result in considerable

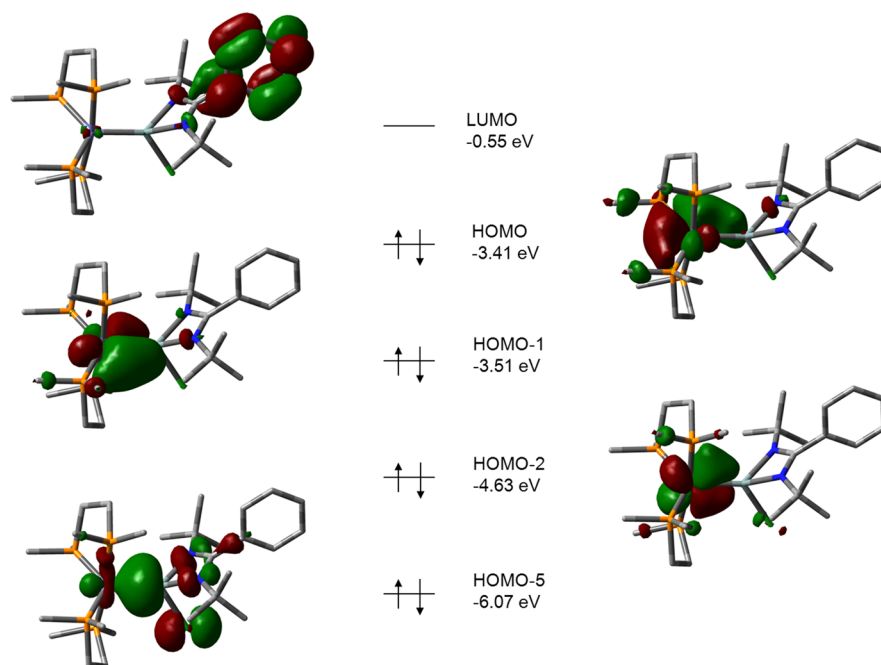


Figure 6. Calculated boundary surfaces of some key frontier MOs and their respective energies of complex 3. Complex 4 was found to exhibit analogous frontier MOs.

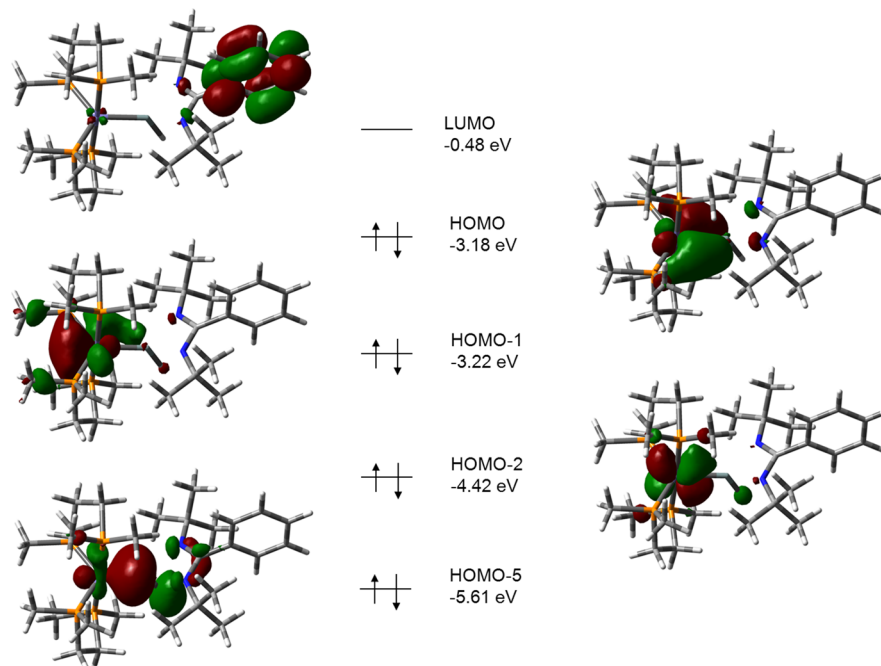


Figure 7. Calculated boundary surfaces of some pertinent frontier MOs and their energies of complex 5. The ligand facilitates better π -back-donation from $\text{Fe}^0 \rightarrow \text{Si}^{\text{II}}$ seen in the HOMO compared to that of 3 and 4.

electron depletion, although DFT calculations on these systems have not been reported. Finally, the HOMO-5 reflects the $\text{Si}^{\text{II}} \rightarrow \text{Fe}^0$ σ -donation, which is also heavily polarized toward the Si^{II} center. The LUMO in complexes 3 and 4 is centered on the phenyl ring of the NHSi ligand. Complex 5 on the other hand exhibits slightly different frontier orbitals in comparison to the other two complexes, most likely due to the small size of the H substituent on the Si^{II} center (Figure 7). Of particular interest is the HOMO orbital, which resembles a more symmetric π -back-donation from the $\text{Fe}^0 \rightarrow \text{Si}^{\text{II}}$ (Figure 8). This can account for

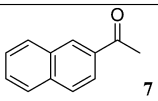
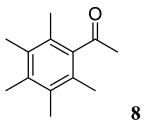
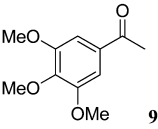
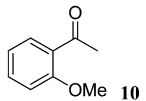
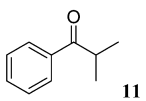
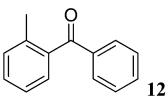
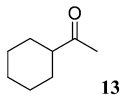
the reduced positive charge on the Si^{II} center, found in the NBO analysis. Moreover, this subtle difference represented by the HOMO in 5 can also account for the earlier observation of a higher energy barrier of Berry pseudorotation observed spectroscopically, *vide supra*. A better $\text{Fe}^0 \rightarrow \text{Si}^{\text{II}}$ π -back-bond would result in electron depletion at the Fe^0 center, which might force stronger coordination of the electron pushing alkylphosphane ligands, accounting for their increased rigidity in solution compared to complexes 3 and 4. As with complexes 3 and 4, the HOMO-5 is seen to exhibit the $\text{Si}^{\text{II}} \rightarrow \text{Fe}^0$ σ -

donation, which is also polarized toward the Si^{II} center (Figure 6), with the LUMO centered on the phenyl ring of the NHSi ligand.

Catalytic Hydrosilylation of Ketones with 5. Over the past few years, iron catalysis has received considerable attention as an alternative to that by precious and toxic metals (e.g., Rh, Ir, Ru) owing to its abundance and low cost.^{35–38} In this regard, excellent performances with Fe precatalysts have been demonstrated in redox chemistry. Moreover, it has been shown that the ligand sphere is of crucial importance for achieving excellent catalytic activities and selectivities. Consequently, we were interested in the evaluation of the catalytic abilities of complex **5** in ketone hydrosilylation chemistry, particularly since no studies have been reported on catalytically active iron–silylene complexes to date. Moreover, no previously reported catalytic studies mediated by a reactive Si(II) hydride have been reported, further precipitating our interest. In the presence of catalytic amounts of **5** (5 mol %), a variety of ketones bearing different steric and electronic properties (7–13) were converted, nearly in all cases in excellent yields to the corresponding alcohols (7a–13a) applying (EtO)₃SiH as a hydrosilane source (Table 5). In one case we even tested the ability of **5** to perform the catalytic hydrosilylation of ketone **9** at ambient temperatures and found that quantitative conversion is even observed without heating. These results are at least comparable to some modern benchmark systems for other iron-based catalytic ketone hydrosilylations.³⁷

To gain insights into the mechanism affecting these hydrosilylation reactions, the reaction of **5** with ketone **7**, in the absence of (EtO)₃SiH, was carried out on preparative scale in the hope of isolating the adduct [(dmpe)₂HFe←{Si←[:O=C(CH₃)(naphthyl)]L}] (**14**), which is a likely first step in the catalytic process. Despite several efforts the product could not be isolated, so the formation of the emerging product was monitored and analyzed by ¹H and ³¹P{¹H} NMR spectroscopy over time. Heating of a sample of **5** with a stoichiometric amount of ketone **7** in toluene-*d*₈ revealed the selective formation of a new iron hydride species, featuring a broad multiplet signal at δ −13.94 ppm, typical of an terminal iron hydride, which is clear evidence of H migration from the silicon to the iron center. The thermal stability of **5** was independently checked in the absence of ketone. In fact, no H-migration from Si to Fe occurs even upon prolonged heating, which supports that the hydride transfer process is induced by ketone coordination to the silicon(II) center. Moreover, monitoring the reaction by ³¹P{¹H} NMR spectra over time revealed the selective formation of two triplet signals at δ 62.2 and 75.7 ppm (²J_{PP} = 27 Hz) along with concomitant consumption of **5**. These data suggest nonrigid stereochemistry, or fluxionality of the formed iron hydride species **14** in accordance with previous observations for some cis-configured Fe–hydrido complexes.³⁹ Attempts at obtaining a ²⁹Si{¹H} NMR spectrum of the emerging product were unsuccessful. Nevertheless, these data provide some evidence for the initial formation of a ketone adduct with concomitant 1,2-H migration from Si to Fe, which is likely the activation step in the catalytic process. Similar observations for Ru-based systems featuring Schrock or Fischer type silylenes had been observed very recently by Tilley and co-workers⁴⁰ and Tobita and co-workers⁴¹ for similar stoichiometric reactions with ketones, further lending supporting this hypothesis.

Table 5. Probing the Catalytic Ability of Complex 5 for Hydrosilylation of Ketones

$\text{R}^1\text{C}(=\text{O})\text{R}^2 \xrightarrow[\text{THF, 70 } ^\circ\text{C, 24 h, work up}]{\text{5 mol\% } \mathbf{5}, \text{1.5 equiv. (EtO)}_3\text{SiH}} \text{R}^1\text{CH}(\text{OH})\text{R}^2$		
Entry	Substrate	Yield [%] ^[b]
1		7a : 92
2		8a : 73
3		9a : 97 9a : >99 ^[c]
4		10a >99
5		11a : 98
6		12a : 98
7		13a : 95

^aReaction conditions: precatalyst (5.0 mol %), substrate (0.16 mmol), (EtO)₃SiH (0.24 mmol), 70 °C, 24 h. ^bYield determined by GC-MS, using *n*-dodecane as internal standard. ^cCatalytic reaction repeated with use of precatalyst (5.0 mol %), substrate (0.16 mmol), (EtO)₃SiH (0.24 mmol), 25 °C, 24 h.

Moreover, the appearance of the proposed intermediate **14** is supported by DFT calculations where it was found to be a minimum on the potential energy hyper surface (Figure 8).

The geometry optimized structure of the simplified model of **14'** reveals a distorted octahedral coordination geometry around the iron center with a terminal hydride ligand, originating from the Si center in **5**. The oxygen atom of the ketone is coordinated to the silicon center and features a Si–O bond length of 1.6427 Å and a C–O bond distance of 1.4495 Å. The latter parameter indicates substantial elongation from a C=O double bond in the free ketone to single bond character, which is the likely source of the C=O bond activation. The Fe–Si bond distance of 2.342 Å is notably longer than is the calculated and experimentally determined value in complex **5** (Table 6), indicating Fe–Si single bond character. Noteworthy is the substantial increase in the NBO charge on the silicon atom in **14'** compared to **5** (Table 6), which suggests **14** can be

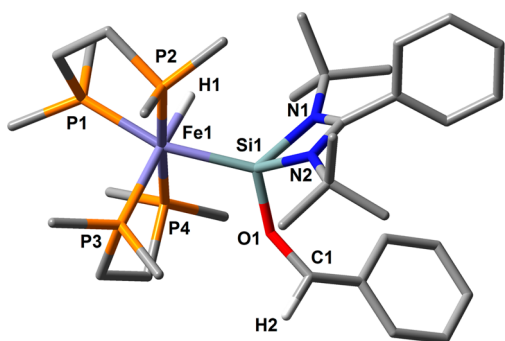


Figure 8. Geometry optimized structure of a simplified model **14'**, using the aldehyde HC(=O)Ph as a likely intermediate in the hydrosilylation of ketones. All H atoms except the Fe–H and the H atom on the aldehyde were omitted for clarity.

Table 6. Comparison of Wiberg Bond Indices (WBI) Values and the Calculated Fe–Si Distances^a of Complexes **5** and **14'**

complex	NBO charge		WBI	Fe–Si distances (Å)
	Fe	Si		
5	−2.198	+1.237	1.1585	2.1976
14'	−2.026	+1.935	0.864	2.342

^aLevel of theory: B3LYP/6-31G(d) for C, H, N, Cl and Si; LANL2DZ for Fe.

considered a betaine-like silyliumylidene– Fe^0 hydride complex bearing a cationic NHSi (silyliumylidene) ligand,⁴² which is stabilized by a dative coordination from the lone pairs on the oxygen atom of the ketone.

Based on these collective findings, a possible mechanism for the hydrosilylation of ketones mediated by **5** could follow a scenario presented in Scheme 3. The coordination of the

ketone to the silicon(II) center results in 1,2-hydride migration to iron affording the betaine-like silyliumylidene– Fe^0 hydride complex featuring an activated $\text{C}=\text{O}$ bond of the ketone. The reaction with the $(\text{EtO})_3\text{SiH}$ likely follows this activation step affording the desired silylated product and reformation of **5** (Scheme 3). The details of the last step of the proposed sequence are currently under investigation.

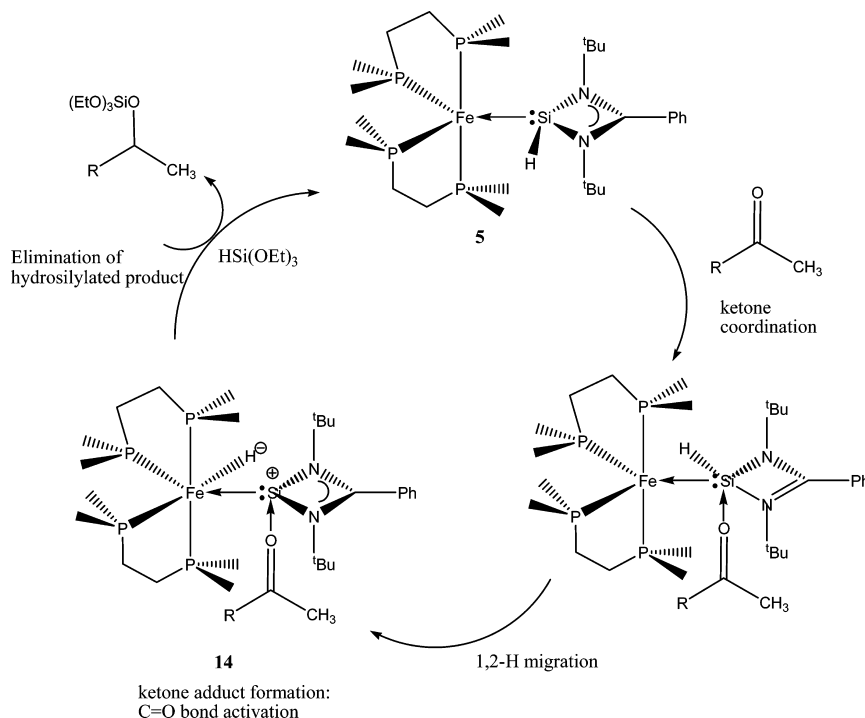
SUMMARY AND CONCLUSIONS

A facile entry to the first electron-rich iron NHSi complexes has been reported. This includes straightforward access to an unprecedented Si^{II} hydride stabilized by an electron-rich $\{\text{FeP}_4\}$ fragment (**5**) by $\text{Cl} \rightarrow \text{H}$ exchange. All complexes show multiple bonding character between the iron and the silicon atom of the NHSi ligand, enhanced by the electron pushing alkylphosphane donor ligands. This is particularly true in the case of the Si^{II} –hydride complex **5**, featuring a classical π -back-bond. Moreover, the first catalytic study of any iron-based NHSi complex or any Si^{II} hydride complex has been reported employing complex **5** as a precatalyst. In this context **5** was found to effectively catalyze the hydrosilylation of a variety of ketones. The NHSi ligand appears to play a key role in this process, and the first step is likely a ketone-mediated 1,2-H migration from Si^{II} to Fe^0 . These findings indicate for the first time that Si^{II} hydride complexes might emerge as a new class of catalysts, by taking advantage of the reactive Si^{II} center in substrate activation. Further experimental and theoretical studies on this and other potential catalytic processes mediated by **5** are currently underway.

EXPERIMENTAL SECTION

General Considerations. All experiments and manipulations were carried out under a dry and oxygen-free atmosphere of nitrogen or argon, using standard Schlenk techniques or in an MBraun inert atmosphere drybox containing an atmosphere of purified nitrogen.

Scheme 3. Proposed Catalytic Cycle for the Hydrosilylation of Ketones by Complex **5**



Solvents were dried by standard methods and stored over LiAlH₄. Prior to use all solvents were recondensed and degassed at least once via a freeze–pump–thaw cycle. C₆D₆ was stirred over excess K₂CO₃ for 48 h, recondensed, and degassed once via a freeze–pump–thaw cycle and stored over activated molecular sieves (4 Å) for use. Complex **1** was prepared by the reduction of [FeCl₂(dmpe)₂]⁴³ according to a published method by Filippou,¹⁹ while the N-heterocyclic chlorosilylene (**2**) was prepared according to the method by Roesky and co-workers.²¹ MeLi was bought from Acros chemical company as a 1.6 M solution in hexane and used as received. Free dmpe and LiBHEt₃ (1 M solution in THF) were obtained from Sigma-Aldrich and used as received. The NMR spectra were recorded on a Bruker AV 200 or 400 spectrometer. Concentrated solutions of samples in C₆D₆ were sealed off in a Young-type NMR tube for measurements. The ¹H and ¹³C{¹H} were referenced to the residual solvent signals as internal standards (δ_{H} 7.15 ; δ_{C} 128.0 ppm for C₆D₆). The ²⁹Si{¹H} NMR spectra were referenced to TMS (tetramethylsilane) as an external standard and ³¹P{¹H} spectra were also externally calibrated with H₃PO₄ in sealed capillaries. Abbreviations: s = singlet; m = multiplet; br = broad, quint = quintet. Unambiguous signal assignments were made by employing a combination of 2D NMR H,H–COSY and H,C–COSY (HMOC, HMBC) experiments. The PCH₂CH₂P are diastereotopic and indicated by X or Y as superscripts in the ¹H NMR spectra. In addition, the methyl groups on the phosphorus atoms of the dmpe ligands are also diastereotopic and indicated by the superscripts A, B, C, or D, respectively. Melting points were determined on an electronic “Melting point tester” device from BSGT company and are uncorrected. For this purpose samples were sealed off in capillaries under nitrogen and heated slowly to observed decomposition or melting. High resolution ESI mass spectra were recorded on an Orbitrap LTQ XL of Thermo Scientific mass spectrometer and the raw data evaluated using the X-calibur computer program. In all cases the isotope distribution pattern of the [M + 1]⁺ signal was checked against theory and the value reported is the line of highest intensity.

Synthesis of [(dmpe)₂Fe(←:Si(Cl)L)] (3**).** A Schlenk tube was charged with **1** (0.100 g, 0.231 mmol) and **2** (0.068 g, 0.231 mmol). The solids were rapidly stirred in a –30 °C bath, and 20 mL of diethyl ether which was also precooled to –30 °C was added to the mixture via cannula. The reaction was taken out of the bath and stirred at room temperature for 2 h during which a dark red solution with the formation of a small amount of colorless precipitate is observed. An in situ ³¹P{¹H} NMR spectrum of an aliquot of the reaction solution at this point showed complete consumption of **1**, the formation of free PMe₃ (δ –60 ppm) and a new broad signal at δ 60 ppm. The reaction solution was filtered via cannula and the red supernatant solution concentrated to ca. 1 mL and cooled to –78 °C. The formation of an orange precipitate was observed, and the light orange supernatant was separated by syringe from this solid. The orange solid was dried in vacuo at room temperature for 1 h resulting in the highly air and moisture sensitive complex **3** (0.121 g, 81%). Crystals suitable for X-ray diffraction analysis were obtained by dissolving a small portion of **3** in diethyl ether and slow cooling to –30 °C for several days; mp 143–146 °C dec. ¹H NMR (400 MHz, C₆D₆, 298 K): δ 1.31 ppm (br s $\Delta\nu_{1/2}$ = 7.1 Hz, 12H, 4 × CH₃^A), 1.33 (s, $\Delta\nu_{1/2}$ = 1.6 Hz, 18H, 2 × NC(CH₃)₃), 1.60 (m, 4H, 4 × PCH^XH^Y), 1.75 (br s $\Delta\nu_{1/2}$ = 7.1 Hz, 12H, 4 × CH₃^B), 1.77 (m, 4H, 4 × PCH^XH^Y) (this signal partially obscured by that at δ 1.75 ppm), 6.84–6.91 (m, 1H, C⁴–H, Ph), 6.91–7.00 (m, 2H, C^{3,5}–H, Ph), 7.20–7.27 (m, 2H, C^{2,6}–H, Ph). ³¹P{¹H} NMR (161.9 MHz, C₆D₆, 298 K): δ 59.8 ppm (br s, $\Delta\nu_{1/2}$ = 58.1 Hz, 2 × dmpe). ¹³C{¹H} NMR (100.6 MHz, C₆D₆, 298 K): δ 25.7 ppm (ps quint, 4C, 4 × CH₃^B), 27.7 (ps quint, 4C, 4 × CH₃^A), 32.5 (s, 6C, 2 × NC(CH₃)₃), 34.7 (quint, ¹J_{PC} = 13.8 Hz, 4C, 4 × PCH^XH^Y), 54.4 (s, 2C, 2 × C(CH₃)₃), 126.6 (s, 1C, 1 × C^{2 or 6}–H, Ph), 127.5 (s, 1C, 1 × C^{3 or 5}–H, Ph), 127.52 (s, 1C, 1 × C⁴–H, Ph), 129.1 (s, 1C, 1 × C^{3 or 5}–H, Ph), 129.9 (s, 1C, 1 × C^{2 or 6}–H, Ph), 134.4 (s, 1C, C¹, Ph), 170.5 (s, 1C, 1 × NCN). ²⁹Si{¹H} NMR (79.5 MHz, C₆D₆, 298 K): δ 43.1 ppm (quint, ²J_{SiP} = 12.1 Hz). ESI-MS, *m/z*: Calcd for [C₂₇H₅₅N₂SiFeP₄Cl + 1]⁺ 651.2196. Found 651.2209.

Synthesis of [(dmpe)₂Fe(←:Si(Me)L)] (4**).** A Schlenk tube was charged with **1** (0.100 g, 0.231 mmol) and **2** (0.068 g, 0.231 mmol) and the two solids were rapidly stirred with cooling to –30 °C. Precooled (to –30 °C) Et₂O (25 mL) was added to the stirring solid mixture rapidly via cannula. The reaction was allowed to stir for 2 h at room temperature generating **3** in situ. The resulting red-orange reaction solution was cooled to –5 °C and MeLi (0.15 mL, 1.6 M solution) was added dropwise to the solution under stirring. An immediate color change to crimson-red is noticed. The reaction was taken out of the cooling bath and stirred at room temperature for a further 1 h. The solvent was removed in vacuo affording a maroon residue, which was extracted with hexane (25 mL). The red hexane filtrate was concentrated to ca. 2 mL and cooled to –30 °C for 2 h. A red solid was isolated by cannula filtration and dried in vacuo at room temperature affording **4** (0.097 g, 67%). Crystals suitable for X-ray diffraction analysis were obtained by dissolving a small portion of **4** in hexane and slow cooling to –30 °C for several days; mp 153–156 °C dec. ¹H NMR (400 MHz, C₆D₆, 298 K): δ 1.04 ppm (s, 3H, 1 × Si–CH₃), 1.21 (s, $\Delta\nu_{1/2}$ = 1.6 Hz, 18H, 2 × NC(CH₃)₃), 1.41 (br s $\Delta\nu_{1/2}$ = 4.9 Hz, 12H, 4 × CH₃^A), 1.65–1.70 (br m, 8H, 4 × PCH^XH^Y + 4 × PCH^XH^Y) (signal partially obscured by that at δ 1.69 ppm), 1.69 (br s $\Delta\nu_{1/2}$ = 5.9 Hz, 12H, 4 × CH₃^B), 6.88–6.93 (m, 1H, C⁴–H, Ph), 6.96–7.02 (m, 2H, C^{3,5}–H, Ph), 7.03–7.07 (m, 1H, C^{2 or 6}–H, Ph), 7.34–7.39 (m, 1H, C^{2 or 6}–H, Ph). ³¹P{¹H} NMR (161.9 MHz, C₆D₆, 298 K): δ 59.1 ppm (br s, $\Delta\nu_{1/2}$ = 48.6 Hz, 2 × dmpe). ¹³C{¹H} NMR (100.6 MHz, C₆D₆, 298 K): δ 25.1 ppm (m, 1C, Si–CH₃), 26.7 (ps quint, 4C, 4 × CH₃^B), 28.3 (ps quint, 4C, 4 × CH₃^A), 32.6 (s, 6C, 2 × NC(CH₃)₃), 35.2 (m, 4C, 4 × PCH^XH^Y), 53.6 (s, 2C, 2 × C(CH₃)₃), 127.10 (s, 1C, 1 × C^{2 or 6}–H, Ph), 127.11 (s, 1C, 1 × C⁴–H, Ph), 127.6 (s, 1C, 1 × C^{3 or 5}–H, Ph), 128.7 (s, 1C, 1 × C^{3 or 5}–H, Ph), 130.4 (s, 1C, 1 × C^{2 or 6}–H, Ph), 135.6 (s, 1C, C¹, Ph), 164.6 (s, 1C, 1 × NCN). ²⁹Si{¹H} NMR (79.5 MHz, C₆D₆, 298 K): δ 102.5 ppm (quint, ²J_{SiP} = 16.1 Hz). ESI-MS, *m/z*: Calcd for [C₂₈H₅₈N₂SiFeP₄ + 1]⁺ 631.2742. Found 631.2726.

Synthesis of [(dmpe)₂Fe(←:Si(H)L)] (5**).** A Schlenk tube was charged with **1** (0.300 g, 0.694 mmol) and **2** (0.210 g, 0.694 mmol) and the two solids were rapidly stirred with cooling to –30 °C. Precooled (to –30 °C) Et₂O (50 mL) was added to the stirring solid mixture rapidly via cannula. The reaction was allowed to stir for 3 h at room temperature generating **3** in situ. The resulting red-orange reaction solution was cooled to 0 °C and Li[BHEt₃] (0.69 mL, 1.0 M thf solution) was added dropwise to the solution under stirring. The reaction was stirred at 0 °C for 20 min then at room temperature for 3 h. At this point in situ ³¹P{¹H} NMR spectroscopy of the reaction solution showed two new signals: at δ –9.2 ppm and a very broad signal δ 60.6 ppm. The solvent was removed in vacuo affording a red-brown residue. A combination of ¹H, ³¹P{¹H}, and ¹¹B{¹H} NMR spectroscopy on a small portion of this residue showed it to be a 1:1 mixture of the desired **5**, and Me₃P→BEt₃ (**6**) resulting from a cross reaction of liberated PMe₃ in the first step of the reaction, and BEt₃ in the second step. The brown residue was extracted into 50 mL of hexane and filtered via cannula then the red-brown solution was concentrated to incipience. It was cooled to –30 °C and a red-brown solid was isolated by careful decantation of the mother liquor. A second crop can be obtained by recooling the mother liquor to –30 °C and decanting the mother liquor, affording **5** as a red-brown solid (0.377 g, 89%). Crystals suitable for X-ray diffraction analysis were obtained by dissolving a small portion of **4** in hexane and slow cooling to –30 °C for several days; mp 131–133 °C dec. ¹H NMR (200 MHz, C₆D₆, 298 K): δ 1.27 ppm (s, $\Delta\nu_{1/2}$ = 5.6 Hz, 18H, 2 × NC(CH₃)₃), 1.44 (br, $\Delta\nu_{1/2}$ = 18.6 Hz, 6H, 2 × CH₃^A), 1.55 (br, $\Delta\nu_{1/2}$ = 24.9 Hz, 8H, PCH₂), 1.65 (br, $\Delta\nu_{1/2}$ = 24.9 Hz, 6H, 4 × CH₃^B), 6.88 (br m, 2H, C⁴–H, Ph + 1 × Si–H signal located by 2D ²⁹Si,H COSY), 6.97 (br m, 2H, C^{3,5}–H, Ph), 7.12 (m, 1H, C^{2 or 6}–H, Ph), 7.31 (m, 1H, C^{2 or 6}–H, Ph). ¹H NMR (400 MHz, C₆D₆, 298 K): δ 1.27 ppm (s, $\Delta\nu_{1/2}$ = 2.7 Hz, 18H, 2 × NC(CH₃)₃), 1.41 (br m, 6H, 2 × CH₃^A), 1.46 (br m, 6H, 2 × CH₃^B), 1.50–1.65 (br m, 8H, 2 × PCH₂CH₂P) (signal partially obscured by that at δ 1.65 ppm), 1.65 (br m, 6H, 4 × CH₃^C), 1.69 (br m, 6H, 4 × CH₃^D), 6.84–6.94 (m, 2H, C⁴–H, Ph + 1 × Si–H signal located by 2D ²⁹Si,H COSY), 6.96–7.02 (m, 2H, C^{3,5}–

H, Ph), 7.12 (m, 1H, C^{2 or 6}-H, Ph), 7.28–7.34 (m, 1H, C^{2 or 6}-H, Ph). ¹H NMR (400 MHz, C₆D₆, 309 K): δ 1.27 ppm (s, Δν_{1/2} = 2.7 Hz, 18H, 2 × NC(CH₃)₃), 1.42 (br m, 12H, 2 × CH₃^{A+B}), 1.50–1.65 (br m, 8H, 2 × PCH₂CH₂P) (signal partially obscured by that at δ 1.65 ppm), 1.65 (br m, 12H, 4 × CH₃^{C+D}), 6.80–6.94 (m, 2H, C⁴-H, Ph + 1 × Si-H), 6.96–7.02 (m, 2H, C^{3,5}-H, Ph), 7.12 (m, 1H, C^{2 or 6}-H, Ph), 7.28–7.34 (m, 1H, C^{2 or 6}-H, Ph). ¹H NMR (400 MHz, C₆D₆, 330 K): δ 1.27 ppm (s, Δν_{1/2} = 2.7 Hz, 18H, 2 × NC(CH₃)₃), 1.42 (br m, 12H, 2 × CH₃^{A+B}), 1.50–1.64 (br m, 8H, 2 × PCH₂CH₂P) (signal partially obscured by that at δ 1.64 ppm), 1.64 (br m, 12H, 4 × CH₃^{C+D}), 6.85 (quint, ³J_{HP} = 9.9 Hz, 1H, Si-H), 6.88–6.96 (m, 2H, C⁴-H, Ph), 6.98–7.04 (m, 2H, C^{3,5}-H, Ph), 7.16 (m, 1H, C^{2 or 6}-H, Ph), 7.28–7.34 (m, 1H, C^{2 or 6}-H, Ph). ¹H NMR (400 MHz, C₆D₆, 340 K): δ 1.27 ppm (s, Δν_{1/2} = 2.7 Hz, 18H, 2 × NC(CH₃)₃), 1.42 (br m, 12H, 2 × CH₃^{A+B}), 1.50–1.65 (br m, 8H, 2 × PCH₂CH₂P) (signal partially obscured by that at δ 1.63 ppm), 1.63 (br m, 12H, 4 × CH₃^{C+D}), 6.84 (quint, ³J_{HP} = 9.9 Hz, 1H, Si-H), 6.88–6.96 (m, 2H, C⁴-H, Ph), 6.98–7.04 (m, 2H, C^{3,5}-H, Ph), 7.16 (m, 1H, C^{2 or 6}-H, Ph), 7.28–7.36 (m, 1H, C^{2 or 6}-H, Ph). ³¹P{¹H} NMR (80.1 MHz, C₆D₆, 298 K): δ 51.5 ppm (v br s, Δν_{1/2} = 1567 Hz). ³¹P{¹H} NMR (161.9 MHz, C₆D₆, 298 K): δ 51.5 ppm (br s, Δν_{1/2} = 1503 Hz, dmpe), 67.9 (br s, Δν_{1/2} = 1503 Hz, dmpe). ³¹P{¹H} NMR (161.9 MHz, C₆D₆, 309 K): δ 59.5 ppm (br s, Δν_{1/2} = 2236 Hz, dmpe). ³¹P{¹H} NMR (161.9 MHz, C₆D₆, 219 K): δ 59.3 ppm (br s, Δν_{1/2} = 1297 Hz, dmpe). ³¹P{¹H} NMR (161.9 MHz, C₆D₆, 330 K): δ 60.3 ppm (br s, Δν_{1/2} = 902 Hz, dmpe). ¹³C{¹H} NMR (100.6 MHz, C₆D₆, 298 K): δ 24.0 ppm (br m, 2C, 2 × CH₃^D), 27.2 (br m, Δν_{1/2} = 122.9 Hz, 8C, 6 × CH₃^{A+B+C}), 32.9 (s, 6C, 2 × NC(CH₃)₃), 35.9 (br m, 4C, 4 × PCH₂H^Y), 53.8 (s, 2C, 2 × C(CH₃)₃), 127.2 (s, 1C, 1 × C^{2 or 6}-H, Ph), 127.2 (s, 1C, 1 × C⁴-H, Ph), 127.4 (s, 1C, 1 × C^{3 or 5}-H, Ph), 128.0 (s, 1C, 1 × C^{3 or 5}-H, Ph) (observed by solvent peak, located by HMQC spectrum), 128.7 (s, 1C, 1 × C^{2 or 6}-H, Ph), 136.0 (s, 1C, C¹, Ph), 164.8 (s, 1C, 1 × NCN). ²⁹Si{¹H} NMR (79.5 MHz, C₆D₆, 298 K): δ 63.6 ppm (quint, ²J_{SiP} = 23.7 Hz). High resolution ESI-MS, m/z: Calcd for [C₂₇H₅₆N₂SiFeP₄ + 1]⁺ 617.2585. Found 617.2581.

Procedure for the Hydrosilylation of Ketones. In a glovebox (N₂-atmosphere) a Schlenk flask was charged with complex 5 (0.036 mmol, 5.0 mol %), the corresponding ketone (0.72 mmol), and THF (2.0 mL). The flask was removed from the glovebox and (EtO)₃SiH (0.79 mmol) was added by syringe. The reaction mixture was stirred in a preheated oil bath at 100 °C for 24 h. The mixture was cooled in an ice bath and was treated with dodecane (10 μL) as GC standard (for GC analysis) and aqueous sodium hydroxide solution (1.0 mL) with stirring. The reaction mixture was stirred for 60 min at room temperature and was then extracted with diethyl ether (2 × 10.0 mL). The combined organic layers were washed with brine, dried with anhydrous Na₂SO₄, and filtered. *n*-Dodecane (internal standard) was added and an aliquot was removed for GC analysis (30 m Rxi-5 ms column, 40–300 °C). **7a:** MS (EI) *m/z* 172 (6, M+), 154 (51), 129 (26), 76 (18), 63 (10), 40 (100). **8a:** MS (EI) *m/z* 192 (65, M+), 174 (100), 159 (68), 149 (94), 133 (47), 119 (23), 105 (17), 91 (20), 77 (12), 43 (24). **9a:** MS (EI) *m/z* 212 (100, M+), 197 (69), 169 (94), 154 (33), 138 (45), 123 (12), 109 (12), 95 (12), 77 (12), 65 (11), 42 (48). **10a:** MS (EI) *m/z* 152 (27, M+), 137 (100), 107 (82), 94 (16), 77 (32), 65 (14), 50 (11), 43 (17). **11a:** MS (EI) *m/z* 150 (8, M+), 107 (100), 79 (53). **12a:** MS (EI) *m/z* 198 (41, M+), 180 (63), 165 (21), 119 (100), 105 (82), 91 (61), 77 (60), 65 (22), 51 (15). **13a:** MS (EI) *m/z* 128 (1, M+), 110 (19), 95 (21), 82 (65), 67 (47), 55 (58), 45 (100).

Theoretical Calculations. DFT calculations on the complexes 3, 4, and 5 were performed at B3LYP level using 6-31G(d) basis sets of the GAUSSIAN-03 program package. Optimized structure of model compounds were obtained without symmetry constraints.

■ ASSOCIATED CONTENT

● Supporting Information

Details on X-ray crystal structure analyses (including a graphical representation of 4), details of the NMR experiment of 14, selected NMR and HR-ESI-MS spectra of 3–5 as well as

Cartesian coordinates, NBO analyses, and optimized structures and additional MOs of 3–5 and model complex 14'. This material is available free of charge via the Internet at <http://pubs.acs.org>.

■ AUTHOR INFORMATION

Corresponding Author

matthias.driess@tu-berlin.de; shigeyoshi.inoue@tu-berlin.de

Notes

The authors declare no competing financial interest.

■ ACKNOWLEDGMENTS

We are grateful to the Cluster of Excellence UniCat (sponsored by the Deutsche Forschungsgemeinschaft and administered by the TU Berlin) for financial support of this research. We thank Dr. J. D. Epping for help concerning the NMR measurements and Dr. S. Yao and G. Tan for help with the structure solutions of 3 and 4.

■ REFERENCES

- (1) This was the first reported NHSi complex that is reported to be thermolabile and no X-ray data or ²⁹Si NMR data were reported, see: Schmid, G.; Welz, E. *Angew. Chem., Int. Ed. Engl.* **1977**, *16*, 785.
- (2) For a recent and comprehensive review on transition metal NHSi complexes, see: Blom, B.; Stoelzel, M.; Driess, M. *Chem.—Eur. J.* **2013**, *19*, 40.
- (3) (a) Meltzer, A.; Präsang, C.; Driess, M. *J. Am. Chem. Soc.* **2009**, *131*, 7232. (b) Meltzer, A.; Inoue, S.; Präsang, C.; Driess, M. *J. Am. Chem. Soc.* **2010**, *132*, 3038. (c) Amoroso, D.; Haaf, M.; Yap, G. P. A.; West, R.; Fogg, D. E. *Organometallics* **2002**, *21*, 534.
- (4) Stoelzel, M.; Präsang, C.; Inoue, S.; Enthaler, S.; Driess, M. *Angew. Chem., Int. Ed.* **2012**, *51*, 399.
- (5) Campion, B. K.; Heyn, R. H.; Tilley, T. D. *J. Chem. Soc., Chem. Commun.* **1988**, 278.
- (6) Wang, W.; Inoue, S.; Enthaler, S.; Driess, M. *Angew. Chem., Int. Ed.* **2012**, *51*, 6167.
- (7) Fürstner, A.; Krause, H.; Lehmann, C. W. *Chem. Commun.* **2001**, 2372.
- (8) Zhang, M.; Liu, X.; Shi, C.; Ren, C.; Ding, Y.; Roesky, H. W. *Z. Anorg. Allg. Chem.* **2008**, *634*, 1755.
- (9) Brück, A.; Gallego, D.; Wang, W.; Irran, E.; Driess, M.; Hartwig, J. F. *Angew. Chem., Int. Ed.* **2012**, *51*, 11478.
- (10) See as selected examples: (a) Azhakar, R.; Ghadwal, R. S.; Roesky, H. W.; Hey, J.; Stalke, D. *Chem. Asian J.* **2012**, *7*, 528. (b) Schmedake, T. A.; Haaf, M.; Paradise, B. J.; Millevolte, A. J.; Powell, D. R.; West, R. *J. Organomet. Chem.* **2001**, *636*, 17. (c) Ramachandran, A.; Sarish, S. P.; Roesky, H. W.; Hey, J.; Stalke, D. *Inorg. Chem.* **2011**, *50*, 5039. (d) Tavcar, G.; Sen, S. S.; Azhakar, R.; Thorn, A.; Roesky, H. W. *Inorg. Chem.* **2010**, *49*, 10199.
- (11) Azhakar, R.; Ghadwal, R. S.; Roesky, H. W.; Wolf, H.; Stalke, D. *J. Am. Chem. Soc.* **2012**, *134*, 2423.
- (12) Neumann, E.; Pfaltz, A. *Organometallics* **2005**, *24*, 2008.
- (13) Gehrhuis, B.; Hitchcock, P. B.; Lappert, M. F.; Maciejewski, H. *Organometallics* **1988**, *17*, 5599.
- (14) (a) Perti, S. H. A.; Eikenberg, D.; Neumann, B.; Stammeler, H.-G.; Jutz, P. *Organometallics* **1999**, *18*, 2615.
- (15) (a) Herrmann, W. A.; Härter, P.; Gstöttmayr, C. W. K.; Bielert, F.; Seeboth, N.; Sirsch, P. *J. Organomet. Chem.* **2002**, *649*, 141. (b) Zeller, A.; Bielert, F.; Härter, P.; Herrmann, W. A.; Strassner, T. *J. Organomet. Chem.* **2005**, *690*, 3292.
- (16) Blom, B.; Driess, M.; Gallego, D.; Inoue, S. *Chem.—Eur. J.* **2012**, *18*, 13355.
- (17) Yang, W.; Fu, H.; Wang, H.; Chen, M.; Ding, Y.; Roesky, H. W.; Jana, A. *Inorg. Chem.* **2009**, *48*, 5058.
- (18) Schmedake, T. A.; Haaf, M.; Paradise, B. J.; Millevolte, A. J.; Powell, D. R.; West, R. *J. Organomet. Chem.* **2001**, *636*, 17.

- (19) Complex **1** was first prepared in the laboratory of Prof. Dr. A. C. Filippou (University of Bonn), by the first author of this publication in 2009. For the synthesis and full characterization of **1** and its reactivity to germynes and stannylenes of the type RECl (E = Ge or Sn, R = 2,6-Mes₂-C₆H₃ or 2,6-Trip₂-C₆H₃; Mes = 2,4,6-Me₃-C₆H₂, Trip = 2,4,6-ⁱPr₃-C₆H₂) see: Blom, B., *Reactivity of Ylenes at Late Transition Metal Centers*, Cuvillier Verlag, 2011, Doctoral thesis, University of Bonn.
- (20) By “silylene complexes” we refer to all types of silylene complexes including the classical Fischer or Schrock type silylene complexes (L_nFe=SiR₂), base stabilized silylene complexes (L_nFe=Si←:DR₂) or NHSi complexes of the type L_nFe←:NHSi.
- (21) (a) So, C.-W.; Roesky, H. W.; Magull, J.; Oswald, R. B. *Angew. Chem., Int. Ed.* **2006**, *45*, 3948. (b) Sen, S. S.; Roesky, H. W.; Stern, D.; Henn, J.; Stalke, D. *J. Am. Chem. Soc.* **2010**, *132*, 1123.
- (22) (a) See also ref 4. (b) Jana, A.; Leusser, D.; Objartel, I.; Roesky, H. W.; Stalke, D. *Dalton Trans.* **2011**, *40*, 5458. (c) Rodriguez, R.; Gau, D.; Contie, Y.; Kato, T.; Saffon-Merceron, N.; Baceiredo, A. *Angew. Chem., Int. Ed.* **2011**, *50*, 11492 and references cited therein. (d) Abraham, M. Y.; Wang, Y.; Xie, Y.; Wei, P.; Schaefer, H. F., III; Schleyer, P. v. R.; Robinson, G. H. *J. Am. Chem. Soc.* **2011**, *133*, 8874. (e) Al-Rafia, S. M. I.; Malcolm, A. C.; McDonald, R.; Ferguson, M. J.; Rivard, E. *Chem. Commun.* **2012**, *48*, 1308 and references cited therein.
- (23) (a) Berry, R. S. *J. Chem. Phys.* **1960**, *32*, 933. (b) Ugi, I.; Marquarding, D.; Klusacek, K.; Gillespie, P. *Acc. Chem. Res.* **1971**, *4*, 288.
- (24) See as examples for similar complexes featuring similar phenomena: (a) Hoffman, P. R.; Miller, J. S.; Ungermann, C. B.; Caulton, K. G. *J. Am. Chem. Soc.* **1973**, *95*, 7902. (b) Ungermann, C. B.; Caulton, K. G. *J. Organomet. Chem.* **1975**, *94*, C9. (c) Komiya, S.; Akita, M.; Yoza, A.; Kasuga, N.; Fukuoka, A.; Kai, Y. *J. Chem. Soc., Chem. Commun.* **1993**, 787. (d) Hirano, M.; Akita, M.; Morikita, T.; Kubo, H.; Fukuoka, A.; Komiya, S. *Dalton Trans.* **1997**, 3453. (e) Matos, R. M.; Verkade, J. G. *J. Braz. Chem. Soc.* **2003**, *14*, 71. (f) Reference 19.
- (25) For an explanation on how measuring frequency affects the NMR time scale see: Bryant, R. G. *J. Chem. Educ.* **1983**, *60*, 933.
- (26) Wilson, S. T.; Coville, N. J.; Shapely, J. R.; Osborn, J. A. *J. Am. Chem. Soc.* **1974**, *96*, 4038.
- (27) A selection of NMR spectra of complexes **3–5** showing these phenomena is available in the Supporting Information, along with crystallographic and DFT data.
- (28) Hansch, C.; Leo, A.; Taft, R. W. *Chem. Rev.* **1991**, *91*, 165.
- (29) Bent, H. A. *Chem. Rev.* **1961**, *61*, 275.
- (30) The τ value is a reflection of the distortion between a perfect square pyramidal geometry ($\tau = 0$) or a perfect trigonal bipyramidal geometry ($\tau = 1$). It can be calculated by using the formula $\tau = (a - b)/60^\circ$, where a and b are the two largest angles. See: Anderson, A. W.; Rao, T. N.; Reedijk, J.; v. Rijn, J.; Verschoor, G. C. *J. Chem. Soc., Dalton Trans.* **1984**, 1349.
- (31) Tobita, H.; Matsuda, A.; Hashimoto, H.; Ueno, K.; Ogino, H. *Angew. Chem., Int. Ed.* **2004**, *43*, 221.
- (32) Basis sets employed: B3LYP/6-31G(d) for C, H, N, Cl and Si; LANL2DZ for Fe. Performed by using Gaussian 03, Revision E.01. See Supporting Information for more full details concerning the DFT calculations of **3–5**.
- (33) Wiberg, K. B. *Tetrahedron* **1968**, *24*, 1083.
- (34) For a concise discussion on bond order and the WBI index for a series of iron silylene and carbene complexes of Fischer and Schrock type, see: Irwin, R. P. *Organometallic Chemistry: Research Perspectives*, 1st ed.; Nova Science Pub Inc.: Hauppauge, NY, 2008; p 292.
- (35) See as examples: (a) Morris, R. H. *Chem. Soc. Rev.* **2009**, *38*, 2282. (b) *Iron Catalysis in Organic Chemistry*; Plietker, B., Ed.; Wiley-VCH: Weinheim, Germany, 2008. (c) Gaillard, S.; Renaud, J.-L. *ChemSusChem* **2008**, *1*, 505. (d) Correa, A.; Mancheño, O. G.; Bolm, C. *Chem. Soc. Rev.* **2008**, *37*, 1108. (e) Sherry, B. D.; Fürstner, A. *Acc. Chem. Res.* **2008**, *41*, 1500. (f) Bullock, R. M. *Angew. Chem.* **2007**, *119*, 7504; *Angew. Chem., Int. Ed.* **2007**, *46*, 7360. (g) Bolm, C.; Legros, J.; Le Pailh, J.; Zani, L. *Chem. Rev.* **2004**, *104*, 6217. (h) Junge, K.; Schröder, K.; Beller, M. *Chem. Commun.* **2011**, *47*, 4849. (i) Bauer, E. B. *Curr. Org. Synth.* **2008**, *12*, 1341. (j) Czaplik, W. M.; Mayer, M.; Cvengros, J.; Jacobi von Wangelin, A. *ChemSusChem* **2009**, *2*, 396. (k) Enthaler, S.; Junge, K.; Beller, M. *Angew. Chem., Int. Ed.* **2008**, *47*, 3317.
- (36) See for instance: (a) Zhang, M.; Zhang, A. *Appl. Organomet. Chem.* **2010**, *24*, 751. (b) Darwish, M.; Wills, M. *Catal. Sci. Technol.* **2012**, *2*, 243. (c) Shaikh, N. S.; Enthaler, S.; Junge, K.; Beller, M. *Angew. Chem., Int. Ed.* **2008**, *47*, 2497.
- (37) Selected references for hydrosilylation of alkynes and ketones with iron catalysts: (a) Bart, S. C.; Lobkovsky, E.; Chirik, P. J. *J. Am. Chem. Soc.* **2004**, *126*, 13794. (b) Haberberger, M.; Irran, E.; Enthaler, S. *Eur. J. Inorg. Chem.* **2011**, 2797. (c) Enthaler, S.; Haberberger, M.; Irran, E. *Chem. Asian J.* **2011**, *6*, 1613. (d) Belger, C.; Plietker, B. *Chem. Commun.* **2012**, *48*, 5419. (e) For a recent review see: Junge, K.; Schröder, K.; Beller, M. *Chem. Commun.* **2011**, *47*, 4849 and references therein. (f) Bezier, D.; Sortais, J.-D.; Darcel, C. *Adv. Synth. Catal.* **2013**, *355*, 19 and references therein.
- (38) References deoxygenation of sulfoxides with iron catalysts: (a) Enthaler, S. *ChemCatChem* **2011**, *3*, 666. (b) Cardoso, J. M. S.; Royo, B. *Chem. Commun.* **2012**, *48*, 4944.
- (39) Meakin, P.; Muetterties, E. L.; Jesson, J. P. *J. Am. Chem. Soc.* **1973**, *95*, 75.
- (40) Fasulo, M. E.; Tilley, T. D. *Organometallics* **2012**, *31*, 5049.
- (41) Ochiai, M.; Hashimoto, H.; Tobita, H. *Organometallics* **2012**, *31*, 527.
- (42) For a recent example of a silyliumylidene, see: (a) Xiong, Y.; Yao, S.; Inoue, S.; Irran, E.; Driess, M. *Angew. Chem., Int. Ed.* **2012**, *51*, 10074. (b) Inoue, S.; Epping, J. D.; Irran, E.; Driess, M. *J. Am. Chem. Soc.* **2011**, *133*, 8514.
- (43) (a) Chatt, J.; Hayter, R. G. *J. Chem. Soc.* **1961**, 5507. (b) Reference 19.